Bull. Chem. Soc. Ethiop. **2025**, 39(3), 571-584.
© 2025 Chemical Society of Ethiopia and The Authors
DOI: https://dx.doi.org/10.4314/bcse.v39i3.14

ISSN 1011-3924
Printed in Ethiopia
Online ISSN 1726-801X

N-DOPED ACTIVATED CARBON DERIVED FROM WATER HYACINTH FOR ULTRA-STABLE METAL-FREE BIFUNCTIONAL ELECTRODE FOR ZINC-AIR BATTERY

Assegid Ergete[1], Yongfa Huang[2], Jiawei Zhou[2], Teklewold Getachew[3], Asmamaw Taye[1], Ruidong Xia[4], Emmanuel Iheanyichukwu Iwuoha[5], Xinwen Peng[2] and Shimelis Admassie[1*]

[1]Department of Chemistry, Addis Ababa University, P.O. Box 1176, Addis Ababa, Ethiopia
[2]State Key Laboratory of Pulp and Paper Engineering, South China University of Technology, Guangzhou 510641, China
[3]Department of Chemistry, Kotebe University of Education, Addis Ababa, Ethiopia
[4]School of Materials Science and Engineering, Nanjing University of Posts and Telecommunications, Nanjing, Jiangsu 210046, China
[5]Key Laboratory for Nano Electrochemistry, University of the Western Cape, Bellville, Cape Town 7535, South Africa

(Received July 11, 2024; Revised November 26, 2024; Accepted December 24, 2024)

ABSTRACT. Activated N-doped carbon derived from water hyacinth leaves (WHL) was prepared and investigated as metal-free bi-functional catalyst for oxygen reduction and evolution (ORR/OER) in zinc-air batteries (ZABs). Scanning electron microscopy (SEM), X-ray photoelectron spectroscopy (XPS) and Brunauer–Emmett–Teller (BET) methods were used to examine the morphology, elemental composition and the specific surface area of the samples, respectively. Linear sweep voltammetry (LSV) at rotating disk electrodes (RDEs) and rotating ring-disk electrodes (RRDEs) were employed to characterize the electrocatalytic activities. The electrochemical studies reveal that N-doped porous carbon from N-WHLs exhibited remarkable electrocatalytic activity for ORR, with an onset potential of 0.95 V and half-wave potential of 0.88 V comparable to commercial Pt/C catalyst. It also displays promising activity towards OER, with an overall potential of 1.86 V versus RHE to reach a current density of 10 mAcm□□, resulting in an oxygen electrode activity (OEA) value of 0.98 V. The percentage of hydrogen peroxide produced was significantly low, with average electron transfer number value of 3.94 at 0.8 V for N-WHL. Furthermore, the ZAB using N-WHL catalysts as an air cathode displayed a power density of 84 mW cm^{-2} and superior stability over 450 hours.

KEY WORDS: Bifunctional catalyst, Oxygen reduction reaction, Oxygen evolution reaction, Water hyacinth, Zinc-air battery

INTRODUCTION

The growing global demand for renewable energy sources such as solar, wind, and hydro has been driven by the diminishing supply of traditional energy sources, as well as the need to reduce greenhouse gas emissions and air pollution [1, 2]. This has spurred the development of technologies that rely on high-performance battery energy storage systems which are critical for harnessing the full potential of the intermittent renewable sources [3]. Among the various energy storage options, lithium-ion batteries (LIBs) are widely used in portable electronics and proposed for electric vehicles. However, their use is limited by concerns over the finite lithium supply, volatile pricing, and safety issues, leading to growing interest in alternative battery chemistries based on more abundant elements like sodium, potassium, magnesium, aluminum, and zinc. Particularly, rechargeable zinc-air batteries (ZABs) hold great promise as an alternative to lithium-ion batteries, offering advantages such as lower cost, higher ambient stability, good compatibility with aqueous electrolytes, non-toxicity, and simplified material processing and

---

*Corresponding authors. E-mail: shimelis.admassie@aau.edu.et battery manufacturing [4, 5]. However, the widespread adoption of zinc-air batteries is hindered by the sluggish kinetics of the oxygen reduction reaction (ORR) and oxygen evolution reaction (OER). These processes require costly, rare, and unstable platinum-based electrocatalysts for ORR and ruthenium/iridium oxide catalysts for OER, which cannot be easily scaled up [6]. Thanks to the 2009 discovery of N-doped carbon nanotubes as effective carbon-based metal-free electrocatalysts (C-MFECs) for the oxygen reduction reaction (ORR), which challenged the necessity of expensive noble metal-based catalysts like platinum (Pt) in fuel cells and metal-air batteries, significant global research efforts have been spurred [7]. Such efficient C-MFECs can also be derived from biomass which is a renewable carbon-rich source. Particularly, utilizing agricultural wastes and invasive plants as feedstock is a more economical approach that supports the development of a sustainable, circular economy [8].

Among the invasive plants, water hyacinth (WH) is one of the worst invasive weeds, causing serious problems in irrigation, navigation, and power generation in many tropical and subtropical countries. To control the spread of this weed, several approaches such as mechanical, chemical, and biological methods have been intensively utilized. However, the most economical approach is to reduce its spread through utilization. Different potential uses for WH have been reported and suggested, such as biomass feedstock, biomethane, bioethanol, organic fertilizer, biogas, remediation for water purification, and sustainable energy applications [7, 9]. Thus, motivated by the method of control via utilization, our research group has intensively investigated and reported on the application of materials derived from water hyacinth for the adsorption of toxic metals like Cr(VI), Pb(II), and Cd(II) ions [10–13]. To further expand the application of materials derived from water hyacinth, we synthesized nitrogen-doped activated carbon from WH and investigated its electrocatalytic activity for both the oxygen reduction reaction (ORR) and the oxygen evolution reaction (OER). This makes it a bifunctional electrocatalyst suitable for use in zinc-air batteries. To the best of our knowledge, there is only one recent report [14] on the use of activated carbon derived from water hyacinth in zinc-air batteries. We found that our synthesized material delivered outstanding stability compared to the previously reported work. The improved stability of the N-WHL material in this study may be attributed to factors such as the different geographical source, pyrolysis methods, and activation agents employed in this work. Here, we present the detailed investigation and the promising results regarding the use of this invasive plant material in zinc-air battery applications.

EXPERIMENTAL

Materials

The water hyacinth leaves (WHL) were collected from Lake Tana, Bahir Dar, Ethiopia. Isopropanol (Sigma-Aldrich, 99.5 wt%), zinc chloride ($ZnCl_2$, 98 wt%), ammonium chloride (NH4Cl, ≥ 99.5%), hydrochloric acid (HCl, 37 wt%), and Nafion® (Aldrich, 5 wt%) solution were provided as analytical grade and used as received. Nitrogen and oxygen gases were purchased in cylinders from Chora Gas and Chemicals Product Factory, Addis Ababa. Deionized water was used in all the experiments.

Synthesis of N-doped porous carbon materials

The water hyacinth leaves (WHL) samples were collected from Lake Tana, Bahir Dar, Ethiopia. The collected leaves were thoroughly cleaned with running water several times and dried in air. The dried leaf part was then crushed to fine powders and pre-carbonized at 500 ºC for 1.0 hour in nitrogen atmosphere. Nitrogen-doped activated carbon derived from water hyacinth leaf (N-WHL-AC) was then prepared by dissolving 4.0 g of $ZnCl_2$ and 1.0 g of NH_4Cl in 50 mL of deionized water followed by the addition of 2.0 g of WHL pre-carbonized at 500 ºC. Then, the mixture was stirred at 25 °C for 8 hours and dried in an oven at 80 ºC for 12 hours. Afterward, the mixture was placed in an atmosphere furnace filled with flowing nitrogen gas and annealed at 800

°C for 1 hour with a heating rate of 10 °C min^{-1}. Finally, the carbon product was collected after being thoroughly washed with 2 M HCl and distilled water and dried at 80 °C. The nitrogen-doped water hyacinth leaves carbon was named N-WHL.

Material characterization

The material morphology was examined with scanning electron microscopy (SEM, SU8600). X-Ray photoelectron spectroscopy (Axis Ultra DLD, Al Kα) was employed to analyze the elemental composition at the surface and the bonding configuration of the samples. N_2 adsorption-desorption isotherms were tested at 77 K using a Micromeritics ASAP 2460 surface area and porosimetry analyzer. The specific surface area (SSA) and pore size distributions (PSD) were determined through the Brunauer-Emmett-Teller (BET) method and a density functional theory (DFT), respectively.

Preparation of N-WHL modified GCE and electrochemical measurements

The electrocatalyst ink for the thin-film electrode was prepared by dispersing 4 mg of N-WHL, 10 µL of Nafion® solution and 1 mL of isopropanol with ultrasonication for 30 min to obtain a homogeneous suspension. 6 µL of this ink was drop-casted on the glassy carbon electrode (diameter 5 mm and collection efficiency, N = 0.37) for RDE measurements. For RRDE measurements, 8 µL of the ink was dropped on the glassy carbon electrodes (diameter 5.61 mm).

All electrochemical measurements were performed using a potentiostat/galvanostat (Autolab PGSTAT 128N) and a Pine bipotentiostat (model AFCBP1) in a three-electrode system where the working electrode is a thin N-WHL film on a glassy carbon electrode. Silver/silver chloride (Ag/AgCl, 3 M KCl) and a platinum wire served as reference and counter electrodes, respectively. The measured potential of this reference electrode was converted to the RHE reference scale using equation (1).

$$\mathrm{E}(V vs.\,\mathrm{RHE}) = \mathrm{E}(V vs.\,\mathrm{Ag/AgCl}) + 0.21\ \mathrm{V} + 0.0591\ \mathrm{V\ x\ pH} \qquad (1)$$

Before testing the electrocatalytic activities of N-WHL for ORR and OER, the electrocatalyst was stabilized using cyclic voltammetry (CV) by scanning the potential between -0.8 V and 0.2 V vs Ag/AgCl at a scan rate of 50 mV s^{-1} for 40 cycles under N_2-purged electrolyte. A 2-cycle CV was then conducted between 0.18 to 1.2 V vs. RHE in 0.1 M KOH at a scan rate of 20 mV s^{-1}.

The ORR activity of N-WHL was evaluated by CV and LSV in an O_2-saturated or an N_2-saturated 0.1 M KOH aqueous solution. A 2-cycle CV measurement was performed between 0.18 to 1.2 V vs. RHE in 0.1 M KOH at a scan rate of 20 mV s^{-1}. RDE LSV measurements were conducted from 0.18 to 1.2 V vs. RHE in 0.1 M KOH at a scan rate of 20 mV s^{-1} under disk rotation rates of 400, 625, 900, 1225, 1600 and 2500 rpm. The apparent number of electrons transferred in the ORR reaction on the carbon catalysts can then theoretically be determined by the Koutecky-Levich equation given by:

$$\frac{1}{J} = \frac{1}{J_L} + \frac{1}{J_K} = \frac{1}{B\omega^{\frac{1}{2}}} + \frac{1}{J_K} \qquad (2)$$

where, $B = 0.2nFC_oD_o^{2/3}\upsilon^{-1/6}$.

The kinetic current density (Jk) can be determined based on mass transfer loss compensation using the equation:

$$J_k = \frac{J_L * J}{J_L - J} \qquad (3)$$

where J is the measured current density, JK is the kinetic current density, JL is the diffusion-limited current density, ω is theelectrode rotation rate, F is the Faraday constant (96485 C mol-1), C0 is the bulk concentration of O_2 (1.2 x 10^{-3} mM), D0 is the diffusion coefficient of O_2 (1.9.x 10^{-5} cm^2 s^{-1}) and υ is the kinetic viscosity of the electrolyte (0.01 cm^2 s^{-1} for 0.1 M KOH solution [9].

For the RRDE test, the disk potential was scanned at 20 mV s^{-1}, and the ring potential was held at 1.5 V vs. RHE in order to oxidize any H2O2 produced [15]. The collection efficiency (N) was determined using 1 M KNO_3 and 10 mM $K_3Fe(CN)_6$ deaerated with pure nitrogen. Equations 4, 5, and 6 were used to calculate the number of electrons transferred during ORR (n), the percentage of H_2O_2 released during ORR, and the collection efficiency of the electrocatalyst, respectively [16].

$$n = \frac{4I_d}{I_d + (I_r/N)} \tag{4}$$

$$\%H_2O_2 = 100\frac{2I_r/N}{I_d + (I_r/N)} \tag{5}$$

$$N = -\frac{I_r}{I_d} \tag{6}$$

where Id is the faradic current at the disk, I_r is the faradic current at the ring, and N is the H_2O_2 collection coefficient at the ring.

For OER measurement, CV and LSV measurements were taken under N_2-purged 0.1 M KOH for a potential range from 0 to 2.1 V for N-WHL (with a catalyst loading of 0.122 gcm^{-2}). For comparison purposes, the ORR and OER catalytic activities of a thin film electrode made from a commercial 20 wt% Pt/C catalyst (30 µg cm^{-2}) were also evaluated under the same conditions.

Fabrication and testing of aqueous rechargeable ZABs

The aqueous rechargeable ZABs were assembled in a two-electrode configuration as per the reference [17]. A polished Zn plate was used as the anode. The electrolyte used for ZABs is a mixed solution of 6 M KOH and 0.2 M $Zn(Ac)_2$. The air cathodes were prepared similarly to the working electrode, except that the GCE was replaced by a carbon cloth with a gas diffusion layer. The mass loading of the catalyst is 1 mg cm^{-2}, and the effective gas diffusion area of the air cathode is 1 cm^2. The charge–discharge cycling test was operated with 5 min for charging and 5 min for discharging at 5 mA cm^{-2} current density by using a Land-CT2001A.

RESULTS AND DISCUSSION

SEM images of the N-WHL sample are shown in Figure 1a-b. The surface morphology of the sample exhibits a randomly oriented granular-like structure with a rough surface; at the same time, in some parts, the catalyst shows a flake like structure. These structures are interconnected with one another and form a porous structure as clearly shown in higher resolution SEM image (Figure 1b). These kinds of structures could offer a high specific surface area with abundant active sites and mass transfer channels [18], which enables the N-WHL sample to be a preferred candidate for bifunctional catalytic performance towards the ORR and OER.

The pore structure and specific surface area of the sample were further quantified by using nitrogen adsorption-desorption measurements. As shown in Figure 1c, the nitrogen adsorption–desorption isotherms and the corresponding pore-size distribution (PSD) of the N-WHL sample were presented. The isotherm of N-WHL displays a joint curve of type I and IV with a distinct hysteresis loop at P/P0 of 0.4 to 1.0, showing a co-existence of micropores and mesopores in the sample (Figure 1d) [9]. The specific surface areas of the porous carbon were characterized by Brunauer-Emmett-Teller (BET) and DFT analysis methods and summarized in Table 1. The

SBET is 794.60 m2 g^{-1} with a total pore volume of 0.42 cm^3/g and a pore diameter of 2.12 nm. Pore size distribution analysis by DFT showed that the sample has a hierarchical porous structure with micropores (< 2 nm) and mesopores (≥ 2 nm) (Figure 1d). Therefore, the results obtained from N_2 adsorption-desorption are in agreement with SEM analysis, where N-WHL has a porous structure. The porous characteristics of N-WHL provide a higher number of active sites that make it more suitable for electron and ion transport [19, 20]. Hence, N-WHL is supposed to be an effective and efficient electrocatalyst material for ORR and OER.

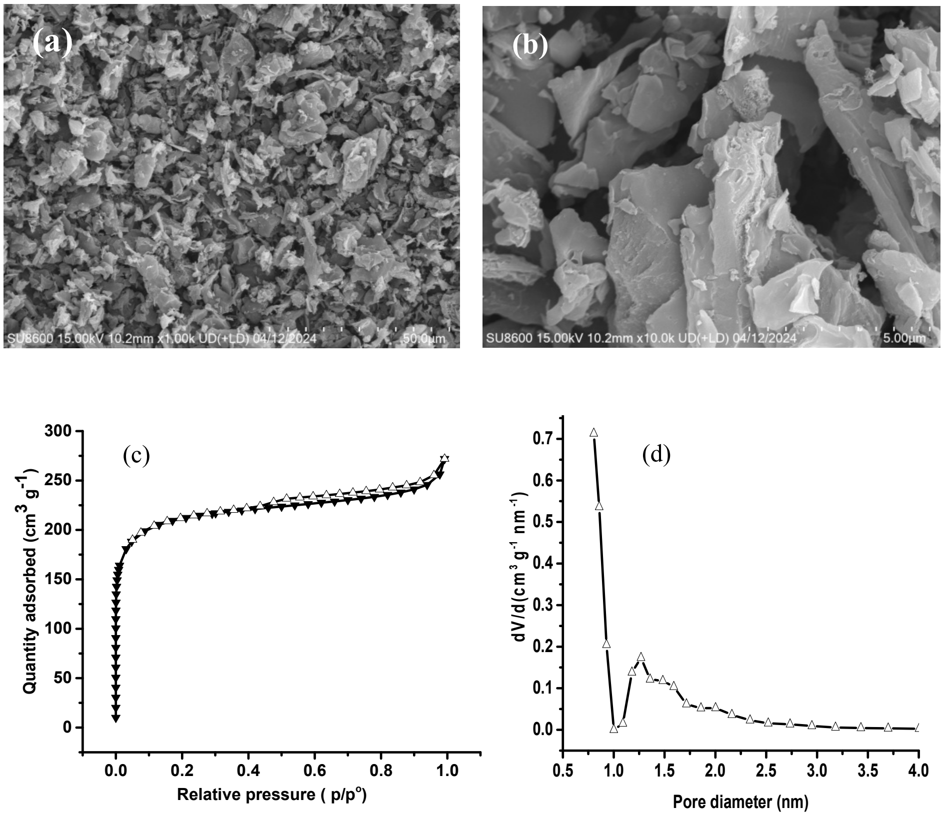

Figure 1. (a) Low magnification (50 µm) and (b) high magnification (5 µm) SEM, (c) N_2 adsorption-desorption isotherm and (d) DFT pore size distribution curve.

The chemical composition and its states in the N-WHL sample were determined using XPS. The survey XPS spectra (Figure 2a and Table 1) displays characteristic peaks at 284.8, 532 and 398.8 eV corresponding to C 1s, O 1s and N 1s, respectively. Moreover, based on the integrated peak areas, N-WHL is primarily constituted of carbon (81.29%), oxygen (11.70 at%), and nitrogen (6.68 at%).

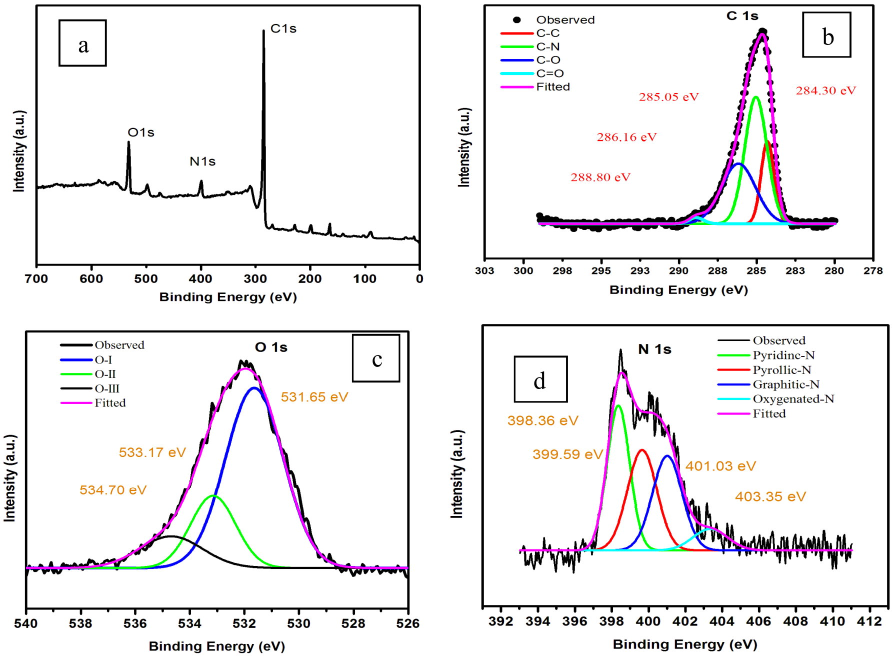

Figure 2. (a) XPS survey spectra of N-WHL; (b) high-resolution XPS spectra of C1s; (c) O1s (c); and (d) N1s.

High-resolution C 1s core level spectrum (Figure 2b) consists of peaks at 284.3 eV, 285.1 eV, 286.2 and 288.8 eV corresponding to C-C, C-N, C-O, and COOH bond, respectively. The deconvoluted O 1s spectrum (Figure 2c) of N-WHL can be resolved into three distinct peaks corresponding to O-I (C=O quinone type groups), O-II (C-OH phenol groups and/or C-O-C ether groups), and O-III (COOH carboxylic groups and/or water), which are respectively assigned to 532.06 eV, 533.17 eV, and 535.25 eV. The survey spectra together with the assigned C-N bond in the deconvoluted C 1s, reveals that the obtained sample was indeed N-doped carbons. The introduction of N facilitates the adsorption and reduction of oxygen, which regulates the electronic characteristics and charge redistribution of C atoms in the carbon skeleton of N-WHL [21, 22]. The catalytic activity of N-doped metal-free carbons with respect to the ORR and OER is influenced especially by the type of N-doping, and its amount as well [23]. The different types of N are further probed by the high-resolution N 1s spectrum of N-WHL (Figure 2d). The spectrum can be divided into four peaks representing pyridinic N, pyrrolic N, graphitic N, and oxidized N, assigned to 398.36, 399.59, 401.03, and 403.35 eV, respectively. The pyridinic N and graphitic N active sites generally govern the ORR, whereas oxygen-containing functional groups and/or p-type doped pyridinic N are the active sites responsible for the OER [24]. As can be seen in Table 1, the contents of pyridinic N and graphitic N in N-WHL are 2.67 and 1.74 at%, respectively. Overall from the physical characterization, the N-WHL synthesized by N-doping pyrolysis is porous and abundantly contains pyridinic N and graphitic N. Thus, N-WHL is expected to exhibit significant electrocatalytic activity towards ORR/OER.

Table 1. Specific surface area (SSA), pore structure, and elemental contents (at%) of NWHL obtained from XPS.

S_{BET} (m^2 g^{-1})	Pore volume (cm^3 g^{-1})	Pore diameter (nm)	C	O	N				
					Pyridinic N	Pyrrolic N	Graphitic N	Oxidized N	Total
794.60	0.42	2.11	81.29	11.70	2.67	1.85	1.74	0.41	6.68

Electrocatalytic activity towards ORR

Electrochemical measurements using cyclic voltammetry and linear sweep voltammetry, together with the hydrodynamic method were performed to assess the electrocatalytic activities of N-WHL towards ORR. Cyclic voltammograms for WHL, N-WHL and Pt/C performed in a 0.1 M KOH solution saturated with N_2 or O_2 are shown in Figure 3a. The WHL and N-WHL show quasi-rectangular voltammograms with no observable peaks in N_2-saturated 0.1 M KOH, while well-defined cathodic peaks were clearly observed at +0.71 V and 0.81 V (+ 0.78 V vs. Pt/C) respectively, in O_2-saturated solution. The anodic shift in the ORR peak potential for N-WHL can be attributed to the nitrogen doping which increases the electron density [25]. This confirms the effective electrochemical reduction of oxygen at WHL and N-WHL. The observed double-layer (capacitive) charging current in WHL and N-WHL in the N_2-saturated electrolyte indicates the existence of good charge propagation throughout the porous carbon framework.

LSV curves (Figure 3b) at 1600 rpm in O_2 saturated KOH for WHL, N-WHL and commercial Pt/C catalysts show consistent results with CV curves. The current density gradually increases over time, rather than exhibiting a sharp rise that leads to saturation as is the case for carbon-based materials [26]. The limiting current density of WHL, N-WHL and Pt/C for O_2 reduction are 2.79, 3.20 and 3.06 $mAcm^{-2}$ at 0.18 V vs RHE. The N-WHL catalyst exhibits a relatively higher limiting current density than WHL and Pt/C. The higher limiting current density for N-WHL could also be attributed to the nitrogen doping known to increase the electron density and surface area. N-WHL exhibited a highly positive half-wave potential ($E_{1/2}$) of +0.88 V that is similar to Pt/C, and a comparable ORR onset potential of $E_o = 0.97$ V to that of Pt/C (0.98 V).

Linear sweep voltammetry at RDE at various rotation speeds (400 to 2500 rpm) was carried out to get further information on the ORR. The polarization curve (Figure 3c) shows the characteristics of the diffusion control region, mixed diffusion kinetic control region, and Tafel region. The corresponding K–L plots (j^{-1} vs $\omega^{-1/2}$) derived from LSV curves are presented in Figure 3c. The K–L plots from +0.70 to +0.80 V are linear and parallel suggesting the first-order reaction kinetics for ORR with respect to the dissolved oxygen concentration [27]. The kinetic current densities (JK) calculated using equation (2) for N-WHL is 1.41 mA cm^{-2} (at 0.80 V vs. RHE) and is highly close to the value deduced for Pt/C (1.80 mA cm^{-2}) under the same experimental conditions. Linear sweep voltammetry measurement at the ring-disk electrode (RRDE) is also performed to evaluate the extent of peroxide formation, the number of electrons transferred per O2 molecules (n) and the ORR pathways. The collection efficiency (N) of the ring was found using equation (6) to be 0.37 for Pt/C and 0.43 for WHL and N-WHL. The 'n' value and the corresponding H_2O_2 production (%) during ORR on WHL, N-WHL and Pt/C electrodes were obtained from equations (4) and (5) over the potential range 0.2 V to 0.8 V and plotted in Figure 3e. The average 'n' value for WHL, N-WHL and Pt/C were found to be 3.44, 3.94 and 3.7, respectively at 0.8 V. The average percentage of H_2O_2 yield was relatively low and less than 15% for N-WHL. The lower percentage of H_2O_2 and higher value of 'n' close to four proves that the dominant ORR pathway is the direct reduction of oxygen to water. This is crucial for selecting an efficient electrocatalytic material for metal-air batteries and fuel cells. These results were consistent with the relatively high calculated jk using equation (3) for ORR at the N-WHL electrode compared to WHL and Pt/C electrodes, which reveals that the N-WHL catalyst exhibits a dominant direct four electron reduction reaction pathway.

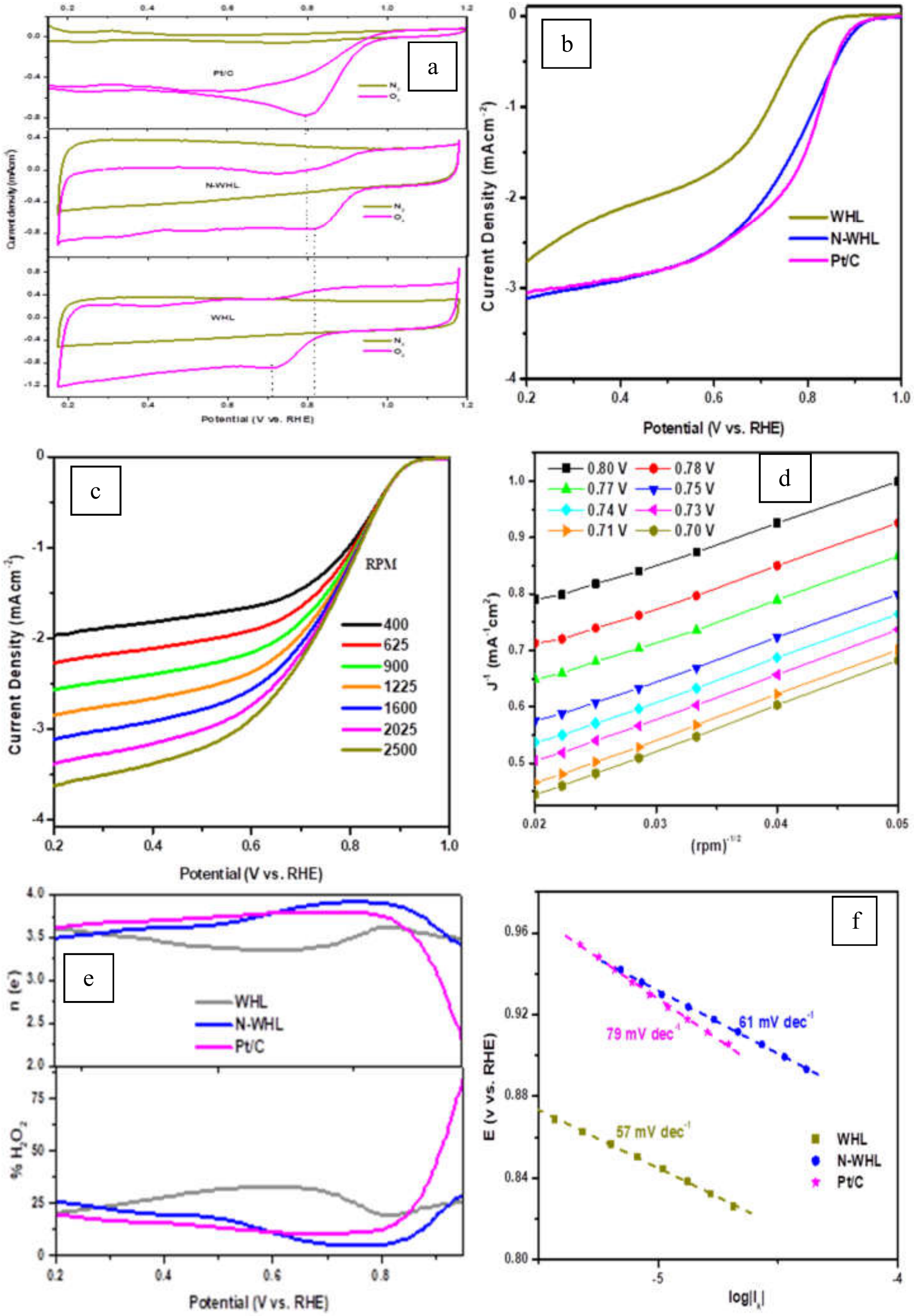

Figure 3. (a) CV curves in N_2- and O_2-saturated solutions for WHL, N-WHL and Pt/C; scan rate: 20 mV s^{-1}; (b) LSV curves in O_2-saturated solutions for WHL, N-WHL and Pt/Cat 1600 rpm and potential scan rate: 10 mV s^{-1}; (c) LSV curves of N-WHL at different rotating

rates; (d)Koutecky–Levich (K–L) plots obtained from LSV curves of N-WHL in O_2-saturated solutions;(e) number of electron transfer (n) and hydrogen peroxide yield (% H_2O_2) at different electrode potential based on RRDE; and (f) Tafel plots for WHL, N-WHL and Pt/C.

To get further insights into the mechanism of the ORR on WHL and N-WHL, Tafel analysis was performed. As shown in Figure 2f, N-WHL exhibited a lower Tafel slope value of 61 mV dec^{-1} than Pt/C (79 mV dec^{-1}). The Tafel slope of N-WHL was comparable and even lower than previously reported carbon-based electro-catalysts (Table S2). This could be due to the presence of a high amount of pyridinic and graphitic N active sites in N-WHL. Hence, the ORR on N-WHL proceeds via a mechanism with a single-electron transfer as the rate-determining step (RDS), indicating more efficient kinetics consistent with a direct four-electron reduction pathway [22].

Table 2. Comparison of ORR catalytic activities for the obtained kinetic parameters (at 0.1 M KOH) of WHL and N-WHL with some biomass-based catalysts in literature.

Sample	OP V vs. RHE	Half-WP V *vs*. RHE	Tafel slope (mV dec^{-1})	Electron number	Mass activity (J_k/m @ V)	Reference
N-WHL	0.95	0.88	61	3.69 (0.2-0.8 V),	11.5 @ 0.8 V	This work
WHC-700	0.98	-	103	3.51-3.82 (0 to 0.85 V)	5.78 @ 0.8 V	[28]
N-MCNs-7-900		-			7.5 @ 0.8 V	[29]
WHCR-Zn	0.93	0.80		3.6 (at 0.5 V)		[30]
SNPC-900	0.97	0.85	58	-	-	[31]
AWC–1	0.92	0.85	55.6	-	-	[31]
WHNC-A		0.84				[14]

Electrocatalytic activity towards OER

The electrocatalytic activities of N-WHL for the OER were assessed in an O_2-saturated 0.1 M KOH solution, as shown in Figure 4a. The polarization curve shows a lower onset potential for the N-WHL sample (1.63 V) and a higher current density compared to the commercial Pt/C (> 1.71 V).

N-WHL catalyst also showed a relatively small overpotential (630 mV) compared to Pt/C (850 mV) at a current density of 10 mA cm^{-2} (J_{10}), exhibiting a superior electrocatalytic activity towards OER. The Tafel plots for OER kinetics were obtained from the LSV measurements (shown in Figure 4a-b). The N-WHL displays an overall lower Tafel slope of 296 mV dec^{-1} than Pt/C (~310 mV dec^{-1}). This could be presumably due to the presence of oxygen-containing functional groups and pyridinic-N active sites. There is a huge range of reported values of Tafel slope for N-doped carbon electrocatalyst materials that lie between 658 mV/dec and 83 mV/dec due to the complexity of the material structures with a variety of reaction mechanisms [32, 33]. The overall ORR/OER activities of the N-WHL electrocatalyst were evaluated using the potential gap ($\Delta E = E_j = 10 - E^{1/2}$) between OER ($E_j = 10$) and ORR ($E_{1/2}$) as shown in Figure 4c. This potential gap is thermodynamically preferred to be narrow and is a key parameter to evaluate the electrocatalytic performance during reversible oxygen catalysis [34]. The N-WHL catalyst showed ΔE of 0.98 V, which is comparable to highly active electrocatalysts including Pt/C (ΔE = 0.94 V) [35], I_r/C (ΔE = 0.92 V) [36], transition metal $CaMn_4O_x$ (ΔE = 1.04 V) [36]; NixOy/N-doped C (ΔE = 0.93 V) [15], and non-metal material (N-doped graphene/carbon nanotubes) (ΔE ≈ 1.00 V) [23].

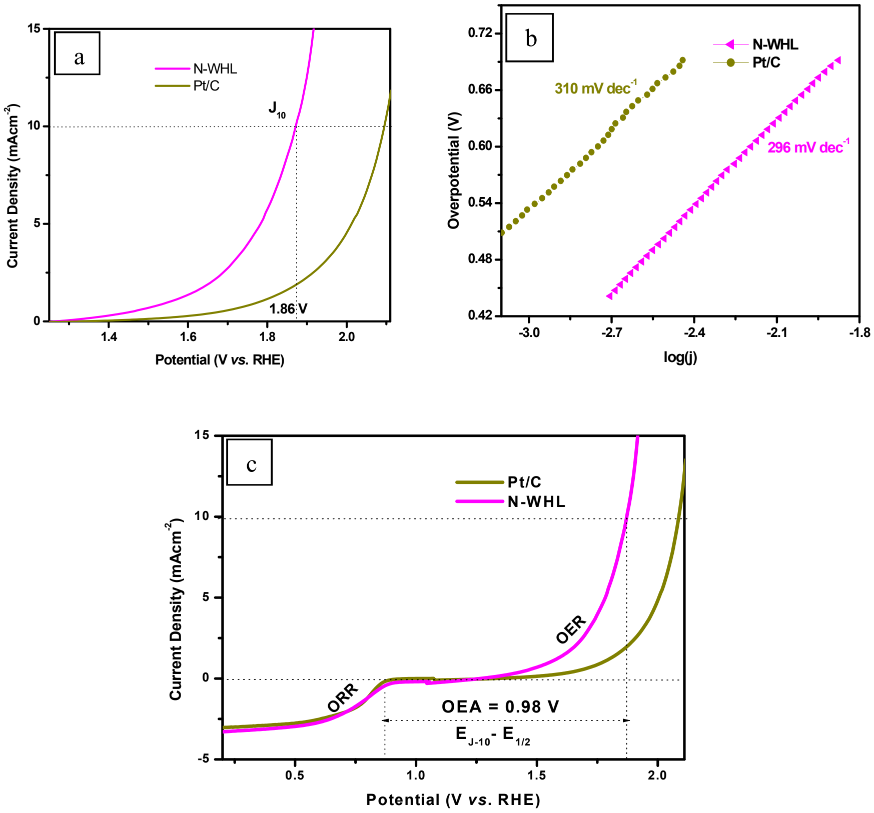

Figure 4. OER Performance: (a) polarization OER curves of N-WHL and commercial Pt/C electrodes;(b) Tafel plots; and (c) the overall polarization curves (ORR + OER) of N-WHL and Pt/C for the potential range of 0.2-2.0 V, in O_2-saturated 0.1 M KOH at 1600 rpm and scan rate of 10 mVs^{-1}.

Performance of aqueous rechargeable ZABs

Considering the promising bifunctional ORR/OER activity of the prepared N-WHL electrocatalyst, the viability of the material for aqueous ZAB as a cathode catalyst was tested in a two-electrode device. Accordingly, the power density polarization and discharging-charging curves (in Figure 5a) show that N-WHL has a slightly greater power density (84 mW cm^{-2}) than Pt/C-RuO_2 (78 mW cm^{-2}) [14].The specific capacity of N-WHL was 782 mAh g^{-1} Zn at a discharge current density of 5 mA cm^{-2} (Figure 5b), which was comparable with similarly reported as shown in Table 3.

The porous structure, and N doping, the presence of graphitized N in the N-WHL electrocatalyst along with its excellent ORR activity, were responsible for better discharge performance in the ZAB [14, 34]. The doped N helps in storing and transporting electrons, and the graphite-N maximizes the carbon electrocatalyst's ability to transport electrons [35].

The discharging stability test of the electrocatalyst in Figure 5c exhibits outstanding rate capability with all discharge voltages notably staying steady and flat; it displays only a small voltage drops the current density increases from 0 to 40 mA cm^{-2}. Furthermore, the voltage was restored to its initial values when the discharging current density of 40 mA cm^{-2} was lowered to a current density of 2 mA cm^{-2}, indicating a prominent multiplicative performance of the cell, which may be related to the high stability exhibited in Figure 5d.

The stability of the rechargeable Zn-air battery was further evaluated by galvanostatic charge–discharge cycling tests at 1 mA cm^{-2}. The N-WHL-based catalyst exhibited outperforming stability of 450 h (2,700 cycles)with capacity decay of only 0.001% per cycle, manifesting a voltage gap less than 0.8 V between the charging and discharging cycle (Figure 5d, inset). Furthermore, the voltage gap for the 5th and 550th ($\Delta E = \Delta E_{550} - \Delta E_5$) charging and discharging cycle (Figure 5d inset) for N-WHL ($\Delta E = 0.71 - 0.70 = 0.01$ V) which is less than that reported ($\Delta E = 0.06$ V) as well as for Pt/C-RuO_2 ($\Delta E = 0.18$ V) [14].The ultra-stability of N-WHL is demonstrated by the lowest value of 0.01 V (Figure 5b), confirming the catalyst's high stability and the characteristics of porous materials responsible for rapid electron/ion channels and transport of active species, which is in agreement with the results of the SEM [14, 34].

The high performance of the N-WHL-based rechargeable Zn-air battery is comparable to or even superior to those devices involving different bifunctional electrocatalysts reported previously (Table 3) [14, 17, 39]. The exhibited electrocatalytic activity is due to the presence of micro/meso pores in N-WHL from the effect of $ZnCl_2$, and N doping that allows for many structural flaws and exposes extra active sites for electrocatalyzed reaction [14, 34]. The higher power density and improved stability can also be attributed to the successful introduction of the N atom into the carbon backbone.

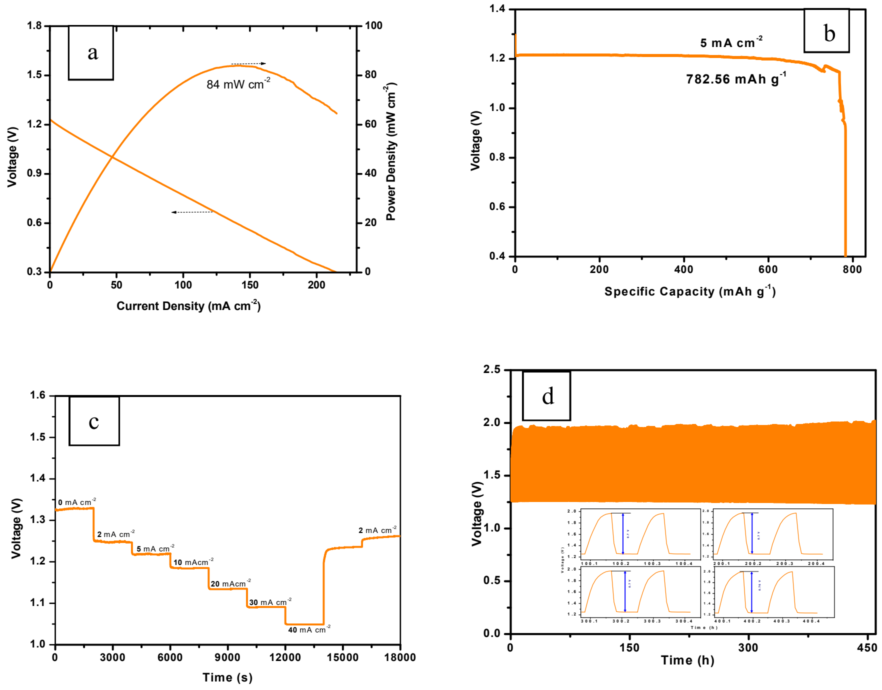

Figure 5. (a) Discharge polarization and power density curves, (b) specific capacity, (c) galvanostatic discharge rate curve and (d) charge–discharge (CD) cycling curves of aqueous rechargeable ZAB of N-WHL, and selected cycles (inset).

Table 3. Comparison of the electrocatalytic activity and ZAB performances of various similar biomass derived catalysts.

Catalyst	ORR and OER performance				ZAB performance			Ref.
	$E_{1/2}$(V) (ORR)	E_{j10} (V) (OER)	ΔE (V)	Tafel (mVdec^{-1}) (ORR)	Activation agent	Specific capacity (mA h/g)/ j(mA/cm^2)	Durability (h)/ j(mA/cm^2)	
WHNC-A	0.843	-	-	92	$ZnCl_2$/ ($C_3H_6N_6$)	775/10	212 /2	[14]
AC-HC	0.77	-	-	50	K_2CO_3/KOH	740.7/10	280/10	[39]
NPBC	0.86	-	-	66	NH_4Cl/NaOH	780/2, 748/10	300/1	[17]
N-WHL	0.88	1.86	0.98	61	$ZnCl_2$/NH_4Cl	782/5	450/1	This work

*Wh g^{-1}.

CONCLUSION

In conclusion, activated N-doped bulk-phase hierarchically porous carbon electrodes were prepared from invasive natural water hyacinth leaves via a facile pyrolysis method using a top-down approach. The carbon-based electrocatalyst N-WHL was evaluated for electrocatalytic reduction and evolution of oxygen as a bifunctional electrocatalyst towards ORR and OER activities, highlighting its potential application for ZABs. Electrochemical measurements of the fabricated N-doped carbon catalyst (N-WHL) showed enhanced catalytic activity for ORR in alkaline media, with remarkable performance that was highly comparable to that of commercial Pt/C catalysts. Due to its cross-linked pore structure, large specific surface area (794.60 m^2 g^{-1}) and nitrogen-rich active sites, N-WHL displays outstanding electrocatalytic ORR/OER performance ($E_{1/2}$ = 0.88 V, E_j = 10 = 1.86 V). The N-WHL electrocatalyst is highly comparable to the best biomass-based carbon catalysts reported in the literature in terms of important kinetic parameters including half-wave potential (0.88 V) and onset potential (0.95 V). Furthermore, the significantly low percentage of hydrogen peroxide produced and electron transfer number values (approximately 3.94 at 0.8 V) indicate a direct 4e$^-$ pathway dominates the ORR activity of N-WHL demonstrating electrocatalytic selectivity. N-WHL also exhibits a good activity towards OER achieving a potential of 1.86 V (vs. RHE) to attain a current density of 10 mAcm$^{-2,}$ with an electrode activity value of 0.98 V. The assembled reversible ZABs demonstrate promising performance, with an acceptable peak power density of (84 mW cm^{-2}), and long-term cycling stability over 450 hours. As a result, the simple, low-cost, and easily scalable synthesis method employed in this work provides insights thoughts for the utilization of value-added biomass and the preparatiaon of bulk-phase porous carbon electrodes for energy-related devices.

ACKNOWLEDGMENT

The financial support from the International Science Program (ISP), Uppsala University, Sweden and Bio and Emerging Technology Institute is greatly acknowledged.

REFERENCES

1. Farghali, M.; Osman, A.I.; Chen, Z.; Abdelhaleem, A.; Ihara, I.; Mohamed, I.M.A.; Yap, P.-S.; Rooney, D.W. Social, environmental, and economic consequences of integrating renewable energies in the electricity sector: A review. *Environ. Chem. Lett.* **2023**, 21, 1381-1418.
2. Gielen, D.; Boshell, F.; Saygin, D.; Bazilian, M.D.; Wagner, N.; Gorini, R. The role of renewable energy in the global energy transformation. *Energy Strat. Rev.* **2019**, 24, 38-50.

3. Zhu, Z.; Jiang, T.; Ali, M.; Meng, Y.; Jin, Y.; Cui, Y.; Chen, W. Rechargeable batteries for grid scale energy storage. *Chem. Rev.* **2022**, 122, 16610-16751.
4. Zhang, N.; Chen, X.; Yu, M.; Niu, Z.; Cheng, F.; Chen, J. Materials chemistry for rechargeable zinc-ion batteries. *Chem. Soc. Rev.* **2020**, 49, 4203-4219.
5. Zhai, S.; Jiang, Z.; Chen, X.; Hui, K.N.; Chen, F. Flexible one-dimensional zn-based electrochemical energy storage devices: Recent progress and future perspectives. *J. Mater. Chem. A* **2021**, 9, 26573-26602.
6. Zhao, Y.; Adiyeri Saseendran, D.P.; Huang, C.; Triana, C.A.; Marks, W.R.; Chen, H.; Zhao, H.; Patzke, G.R. Oxygen evolution/reduction reaction catalysts: from in situ monitoring and reaction mechanisms to rational design. *Chem. Rev.* **2023**, 123, 6257-6358.
7. Hu, C.; Paul, R.; Dai, Q.; Dai, L. Carbon-based metal-free electrocatalysts: From oxygen reduction to multifunctional electrocatalysis. *Chem. Soc. Rev.* **2021**, 50, 11785-11843.
8. Zhang, G.; Liu, X.; Wang, L.; Fu, H. Recent Advances of biomass derived carbon-based materials for efficient electrochemical energy devices. *J. Mater. Chem. A* **2022**, 10, 9277-9307.
9. Morales S, L.; Baas-López, J.M.; Barbosa, R.; Pacheco, D.; Escobar, B. Activated carbon from water hyacinth as electrocatalyst for oxygen reduction reaction in an alkaline fuel cell. *Int. J. Hydrogen Energy* **2021**, 46, 25995-26004.
10. Yifru, A.; Mekonnen, N.; Mehretie, S.; Admassie, S. Polypyrrole–polyaniline-water hyacinth leaf protein concentrate composite for the removal of Cr(VI) from aqueous solution: Kinetics, isotherm and thermodynamic studies. *Bull. Chem. Soc. Ethiop.* **2022**, 36, 571-584.
11. Taye, A.; Mehretie, S.; Getachew, N.; Admassie, S. Adsorption of hexavalent chromium on koh activated carbon derived from water hyacinth leaf coated with polyaniline/polypyrrole. *Sinet: Ethiop. J. Sci.* **2024**, 46, 223-236.
12. Taye, A.; Mehretie, S.M.; Admassie, S. Adsorption of lead(II) ions using KOH-activated carbon derived from water hyacinth. *Bull. Chem. Soc. Ethiop.* **2023**, 37, 1369-1382.
13. Taye, A.; Yifru, A.; Getachew, N.; Mehretie, S.; Admassie, S. Adsorption of hexavalent chromium using water hyacinth leaf protein concentrate/graphene oxide hydrogel. *Environ. Monit. Assess.* **2023**, 195, 1342-1350.
14. Shi, K.; Li, Y.; Zhang, Y.; Li, X.; Zhu, Z.; Xu, H.; Zheng, L.; Gao, J. N-Doped 3D hierarchical carbon from water hyacinth for high-performance zn-air batteries. *Diam. Relat. Mater.* **2023**, 135, 109841-109850.
15. Zheng, Y.; Jiao, Y.; Ge, L.; Jaroniec, M.; Qiao, S.Z. Two-step boron and nitrogen doping in graphene for enhanced synergistic catalysis. *Angew. Chem. Int. Ed.* **2013**, 52, 3110-3116.
16. Getachew, T.; Addis, F.; Mehretie, S.; Yip, H.-L.; Xia, R.; Admassie, S. Electrocatalytic reduction of oxygen at platinum nanoparticles dispersed on electrochemically reduced graphene oxide/PEDOT:PSS composites. *RSC Adv.* **2020**, 10, 30519-30528.
17. Cui, P.; Li, T.; Chi, X.; Yang, W.; Chen, Z.; Han, W.; Xia, R.; Shimelis, A.; Iwuoha, E.I.; Peng, X. Bamboo derived n-doped carbon as a bifunctional electrode for high-performance zinc–air batteries. *Sustain. Energy Fuels* **2023**, 7, 2717-2726.
18. Wu, Z.; Song, M.; Wang, J.; Liu, X. Recent progress in nitrogen-doped metal-free electrocatalysts for oxygen reduction reaction. *Catal.* **2018**, 8, 196-207.
19. Oh, T.; Ryu, S.; Oh, H.; Kim, J. $MnCo_2O_4$ nanoparticles supported on nitrogen and sulfur co-doped mesoporous carbon spheres as efficient electrocatalysts for oxygen catalytic reactions. *Dalton Trans.* **2019**, 48, 945-953.
20. Xu, M.; Huang, Q.; Lu, J.; Niu, J. Green synthesis of high-performance supercapacitor electrode materials from agricultural corncob waste by mild potassium hydroxide soaking and a one-step carbonization. *Ind. Crop. Prod.* **2021**, 161, 113215-113222.
21. Hu, C.; Dai, L. Doping of carbon materials for metal-free electrocatalysis. *Adv. Mater.* **2019**, 31, 1804672-1804686.
22. Kaare, K.; Yu, E.; Volperts, A.; Dobele, G.; Zhurinsh, A.; Dyck, A.; Niaura, G.; Tamasauskaite-Tamasiunaite, L.; Norkus, E.; Andrulevičius, M.; Danilson, M.; Ivar

Kruusenberg, I. Highly active wood-derived nitrogen-doped carbon catalyst for the oxygen reduction reaction. *ACS Omega* **2020**, 5, 23578-23587.

23. Tian, G.; Zhao, M.; Yu, D.; Kong, X.; Huang, J.; Zhang, Q.; Wei, F. Nitrogen-doped graphene/carbon nanotube hybrids: in situ formation on bifunctional catalysts and their superior electrocatalytic activity for oxygen evolution/reduction reaction. *Small* **2014**, 10, 2251-2259.
24. Chen, Y.; Shen, L.; Wang, C.; Feng, S.; Zhang, N.; Xiang, S.; Feng, T.; Yang, M.; Zhang, K.; Yang, B. Utilizing In-situ polymerization of pyrrole to fabricate composited hollow nanospindles for boosting oxygen evolution reaction. *Appl. Catal. B: Environ.* **2020**, 274, 119112-119119.
25. Li, Y.; Liu, L.; Wu, Y.; Wu, T.; Wu, H.; Cai, Q.; Xu, Y.; Zeng, B.; Yuan, C.; Dai, L. Facile Synthesis of nitrogen-doped carbon materials with hierarchical porous structures for high-performance supercapacitors in both acidic and alkaline electrolytes. *J. Mater. Chem. A* **2019**, 7, 13154-13163.
26. Hu, C.; Dai, Q.; Dai, L. multifunctional carbon-based metal-free catalysts for advanced energy conversion and storage. *Cell Rep.* **2021**, 2, 100328-1003243.
27. Liu, X.; Zou, S.; Chen, S. Ordered mesoporous carbons codoped with nitrogen and iron as effective catalysts for oxygen reduction reaction. *Nanoscale* **2016**, 8, 19249-19255.
28. Jafari, N. Ecological and socio-economic utilization of water hyacinth (*Eichhornia crassipes* Mart Solms). *J. Appl. Sci. Environ. Manage.* **2010**, 14, 43-49.
29. Zhang, Z.; Yang, S.; Li, H.; Zan, Y.; Li, X.; Zhu, Y.; Dou, M.; Wang, F. Sustainable carbonaceous materials derived from biomass as metal-free electrocatalysts. *Adv. Mater.* **2019**, 31, 1805718-1805731.
30. Yan, Z.; Dai, C.; Zhang, M.; Lv, X.; Zhao, X.; Xie, J. Nitrogen doped porous carbon with iron promotion for oxygen reduction reaction in alkaline and acidic media. *Int. J. Hydrogen Energy* **2019**, 44, 4090-4101.
31. Zhang, H.; Yan, Y.; Yang, L. Preparation of activated carbon from sawdust by zinc chloride activation. *Adsorption* **2010**, 16, 161-166.
32. Hu, C.; Dai, L. Carbon-based metal-free catalysts for electrocatalysis beyond the ORR. *Angew. Chem. Int. Ed.* 2016, 55, 11736-11758.
33. Wang, L.; Yin, F.; Yao, C. N-Doped graphene as a bifunctional electrocatalyst for oxygen reduction and oxygen evolution reactions in an alkaline electrolyte. *Int. J. Hydrogen Energy* **2014**, 39, 15913-15919.
34. Zhang, J.; Zhang, M.; Zeng, Y.; Chen, J.; Qiu, L.; Zhou, H.; Sun, C.; Yu, Y.; Zhu, C.; Zhu, Z. Single Fe atom on hierarchically porous S, N-codoped nanocarbon derived from porphyra enable boosted oxygen catalysis for rechargeable zn-air batteries. *Small* **2019**, 15, 1900307-1900315.
35. Masa, J.; Xia, W.; Sinev, I.; Zhao, A.; Sun, Z.; Grützke, S.; Weide, P.; Muhler, M.; Schuhmann, W. Mn_xO_y/NC and Co_xO_y/NC nanoparticles embedded in a nitrogen-doped carbon matrix for high-performance bifunctional oxygen electrodes. *Angew. Chem. Int. Ed.* **2014**, 53, 8508-8512.
36. Gorlin, Y.; Jaramillo, T.F. A bifunctional nonprecious metal catalyst for oxygen reduction and water oxidation. *J. Am. Chem. Soc.* **2010**, 132, 13612-13614.
37. Liang, J.; Tang, D.; Huang, L.; Chen, Y.; Ren, W.; Sun, J. High oxygen reduction reaction performance nitrogen-doped biochar cathode: a strategy for comprehensive utilizing nitrogen and carbon in water hyacinth. *Bioresour. Technol.* **2018**, 267, 524-531.
38. Rajasekaran, N.; Vinoba, M.; Al-Sheeha, H.; Rana, M.S. The synergistic character of highly n-doped coconut-shell activated carbon for efficient CO_2 capture. *ChemistrySelect* **2021**, 6, 9149-9156.
39. Feng, J.; Tang, R.; Wang, X.; Meng, T. Biomass-derived activated carbon sheets with tunable oxygen functional groups and pore volume for high-performance oxygen reduction and Zn–air batteries. *ACS Appl. Energy Mater.* **2021**, 4, 5230-5236.